RESEARCH ARTICLE

Quantitative Evaluation of Tumor Early Response to a Vascular-Disrupting Agent with Dynamic PET

Ning Guo,[1] Fan Zhang,[2,3] Xiaomeng Zhang,[1] Jinxia Guo,[2,3] Lixin Lang,[3] Dale O. Kiesewetter,[3] Gang Niu,[3] Quanzheng Li,[1] Xiaoyuan Chen[3]

[1]Center for Advanced Medical Imaging Sciences, Department of Radiology, Massachusetts General Hospital/Harvard Medical School, Boston, MA, 02114, USA

[2]Center for Molecular Imaging and Translational Medicine, State Key Laboratory of Molecular Vaccinology and Molecular Diagnostics, School of Public Health, Xiamen University, Xiamen, China361005

[3]Laboratory of Molecular Imaging and Nanomedicine, National Institute of Biomedical Imaging and Bioengineering, National Institutes of Health, 35A Convent Dr, GD937, Bethesda, MD, 20892-3759, USA

Abstract

Purpose: The purpose of this study is to evaluate the early response of tumors to a vascular-disrupting agent (VDA) VEGF$_{121}$/recombinant toxin gelonin (rGel) using dynamic [^{18}F]FPPRGD2 positron emission tomography (PET) and kinetic parameter estimation.

Procedures: Two tumor xenograft models: U87MG (highly vascularized) and A549 (moderately vascularized), were selected, and both were randomized into treatment and control groups. Sixty-minute dynamic PET scans with [^{18}F]FPPRGD2 that targets to integrin $\alpha_v\beta_3$ were performed at days 0 (baseline), 1, and 3 since VEGF$_{121}$/rGel treatment started. Dynamic PET-derived binding potential (BP$_{ND}$) and parametric maps were compared with tumor uptake (%ID/g) and the static PET image at 1 h after the tracer administration.

Results: The growth of U87MG tumor was obviously delayed upon VEGF$_{121}$/rGel treatment. A549 tumor was not responsive to the same treatment. BP$_{ND}$ of treated U87MG tumors decreased significantly at day 1 ($p<0.05$), and the difference was more significant at day 3 ($p<0.01$), compared with the control group. However, the tracer uptake (%ID/g) derived from static images at 1-h time point did not show significant difference between the treated and control tumors until day 3. Little difference in tracer uptake (%ID/g) or BP$_{ND}$ was found between treated and control A549 tumors. Considering the tracer retention in tumor and the slower clearance due to damaged tumor vasculature after treatment, BP$_{ND}$ representing the actual specific binding portion appears to be more sensitive and accurate than the semiquantitative parameters (such as %ID/g) derived from static images to assess the early response of tumor to VDA treatment.

Conclusions: Quantitative analysis based on dynamic PET with [^{18}F]FPPRGD2 shows advantages in distinguishing effective from ineffective treatment during the course of VEGF$_{121}$/rGel therapy at early stage and is therefore more sensitive in assessing therapy response than static PET.

Key words: Dynamic PET, Vascular-disrupting agent, Integrin $\alpha_v\beta_3$, [^{18}F]FPPRGD2

Introduction

The battle against cancer using conventional therapies, such as chemotherapy and radiotherapy, has been

challenged by the lack of specific targets, which results in mild tumor damage but serious side effects [1]. The failure to detect lesions at early stage, the insufficient damage to cancer targets, and the inability to quantify therapy response are all challenges to achieve curative effects. Instead of attacking the tumor cells directly, which has been proven difficult, an alternative way is to firmly hit the intratumoral targets that are closely associated with tumor cells both functionally and locally. It has been well established that not only the rapid growth of primary tumor but also the maintenance of metastases places tremendous strains on the neovasculature, which shows abnormalities such as rapidly dividing endothelial population, blind ends, leaky vessels, and a reduction in pericytes [2–5]. As a result, angiogenesis has been a major focus of recent cancer research in tumor growth, invasion, and metastasis, prompting the development of numerous vasculature targeted therapies [6].

In recent years, a novel class of vascular-disrupting agents (VDAs) that causes a rapid and selective shutdown of the tumor vessels has been under active investigation [2]. VDAs perturb the tumor vascular endothelial cells, causing loss of morphology, cohesion, and cytotoxicity, leading to selective collapse of the tumor vasculature and subsequent tumor necrosis [7]. The vascular endothelial growth factor (VEGF)/vascular endothelial growth factor receptor (VEGFR) signaling pathway plays a pivotal role in both normal vasculature development and many disease processes [8–11]. The importance of VEGF/VEGFR signaling pathway in cancer is underscored by the approval of the humanized anti-VEGF monoclonal antibody bevacizumab for the first-line treatment of cancer patients [12]. The proangiogenic actions of VEGF/VEGFR pathway are mainly mediated by the cytokine vascular endothelial growth factor-A (VEGF-A) and two endothelium-specific receptor tyrosine kinases, VEGFR-1 (Flt-1/FLT-1) and VEGFR-2 (Flk-1/KDR) [13]. Upregulation/overexpression of the KDR or the VEGF-A ligand itself has been implicated as poor prognostic markers in clinical studies [4]. Thus, many therapeutic agents and approaches targeting the VEGF-A pathway have been developed [14]. We previously characterized a vasculature-targeting fusion protein (VEGF$_{121}$/recombinant plant toxin gelonin (rGel)), a VDA composed of the VEGF-A isoform VEGF$_{121}$ and rGel, in several tumor models [6, 15, 16]. The VEGF$_{121}$/rGel fusion toxin has been shown to be highly specific and cytotoxic for both quiescent and dividing porcine aortic endothelial (PAE) cells expressing VEGFR-2 (KDR), but not cytotoxic for those cells expressing VEGFR-1 (Flt) and normal organs [6].

Conventional assessment of therapy response is usually assessed by magnetic resonance imaging (MRI) or X-ray computed tomography (CT) measurements on the reduction of tumor size. However, many vasculature-targeting agents, either anti-angiogenic or vasculature disrupting, usually yield effects on the tumor microenvironment but not necessarily on the anatomical size change, especially at early stage of the intervention [17]. Therefore, the Response Evaluation Criteria in Solid Tumor (RECIST), which defines complete response (CR) as total tumor regression and partial response (PR) as 30 % reduction in the sum of the longest tumor axes [18]. However, it is insufficient to study molecular therapeutics such as VDAs.

Since VDAs rarely cause tumor shrinkage at early stage of treatment, clinical trials of these agents have used functional biomarkers, including reduction in tumor perfusion, change in tumor cell metabolism, and ultimate cell death to assess the therapy response. Dynamic contrast-enhanced (DCE) MRI and $H_2^{15}O$ positron emission tomography (PET) are the most commonly used noninvasive imaging methods to measure vascular function. However, the requirement of an on-site cyclotron to produce the extremely short-lived ^{15}O isotope limits the use of $H_2^{15}O$/PET to study tumor vasculature [19]. Although K^{trans} derived from DCE-MRI is a reasonable functional biomarker to estimate vasculature perfusion and permeability, the wide use of DCE-MRI in the clinic is still limited by its low sensitivity and poor reproducibility. In our previous studies, multimodality molecular imaging techniques, including bioluminescence imaging (BLI), static MRI, and static PET imaging, have been employed to evaluate the targeting specificity as well as the treatment efficacy of VEGF$_{121}$/rGel [6]. Furthermore, the feasibility of using multiple PET tracers such as [^{18}F]FDG, [^{18}F]FLT, [^{18}F]FMISO, and [^{18}F]FPPRGD2 to evaluate the tumor response to VEGF$_{121}$/rGel treatment in an MDA-MB-435 xenograft model has been demonstrated [16]. Overall, [^{18}F]FPPRGD2, which targets cell adhesion molecule integrin $\alpha_v\beta_3$, has been shown to be a promising PET imaging probe for response evaluation of VEGF$_{121}$/rGel treatment. However, the imaging indices of early changes in tumor microenvironments responding to drugs, such as VDAs, may be disturbed by the tracer retention in the tumor as well as the slow clearance due to damage to tumor vasculature [20]. Consequently, the tumor uptake of RGD peptides derived from static PET images may not be able to truthfully reflect the receptor density in tumor areas.

Dynamic PET and quantitative analysis using kinetic modeling can provide more information about tumor *in vivo* biology by delineating both the temporal and spatial pattern of tracer uptake in the region of interest. Compared with the conventional semiquantitative method such as standardized uptake value (SUV) or percent injected dose per gram of tissue (%ID/g), kinetic parameters are more reliable and accurate due to the independence from both image acquisition time and nonspecific retention in target tissue. [21]. In addition, several potential sources of deviation in the semiquantitative analysis using static images can be mitigated in the kinetic parameter estimation derived from dynamic images [22]. Therefore, we applied dynamic PET and kinetic analysis to quantitatively assess tumor early response in this study and test the feasibility of distinguishing effective from ineffective VDA treatments.

Materials and Methods

Animal and Tumor Models

The highly vascularized U87MG (human glioblastoma) and moderately vascularized A549 (human lung cancer) tumor models were selected for xenograft establishment [23–25]. U87MG cells were cultured in DMEM supplemented with 10 % fetal bovine serum (FBS) as previously described [26]. The A549 cells were cultured in RPMI 1640 medium supplemented with 10 % FBS, 100 IU/ml penicillin, and 100 µg/ml streptomycin (Invitrogen) and in a humidified atmosphere containing 5 % CO_2 at 37 °C. The subcutaneous tumor was established by inoculating 5×10^6 cells into the left shoulder of each female athymic nude mouse at 5–6 weeks of age (Harlan Laboratories). After 2–3 weeks, when the tumors became palpable, the tumor growth would be monitored by measuring the perpendicular axes of the tumor three times a week. The tumor volume was determined by the formula: $V = a \times (b^2)/2$, where a and b are the length and width of each tumor, respectively, in millimeter. The animal experiments were approved by the NIH Clinical Center Animal Care and Use Committee (ACUC). All mice were maintained in a specific pathogen-free facility in accordance with the requirements of the ACUC.

Study Design

Detailed schedule of drug administration and longitudinal PET scans is summarized in Fig. 1a. For each tumor model, the mice were randomized into treatment (n=16 for U87MG, n=8 for A549) and control groups (n=8 for U87MG, n=8 for A549). Two doses of VEGF$_{121}$/rGel (12 mg/kg/dose) were orally given on day 0 (after the baseline PET scans) and day 2, respectively. Saline was used as control vehicle. Each animal underwent pretreatment PET scans followed by the first administration of drug or control vehicle. Posttreatment scans were performed on day 1 and day 3. The animals that belong to the same group underwent dynamic PET scans on the same day. One mouse in each group was scarified after PET scan for the collection of tissue samples and immunohistological staining.

Dynamic Positron Emission Tomography Scan

The tumor-bearing mice underwent PET scans when the tumor volume reached about 200 mm^3 (about 3 weeks after inoculation). [^{18}F]FPPRGD2 was prepared as previously described, and purity of the product was >95 % [27]. Dynamic PET data acquisition was performed on an Inveon microPET scanner (Siemens Medical Solutions). With the assistance of the positioning laser in the system, the mouse was placed at the center of field of view (FOV). Sixty-minute dynamic PET scans were performed after tail vein injection of ~3.7 MBq (100 µCi) of [^{18}F]FPPRGD2 under the isoflurane anesthesia. During the acquisition period, a thermostat-controlled thermal heater was placed to maintain the mouse body temperature at 37 °C. Dynamic PET images were reconstructed by two iterations of three-dimensional ordered-subset expectation maximum (3-D OSEM) with 14 subsets, followed by 18 iterations of maximum a posteriori (MAP) algorithm with a smoothing parameter of 0.1 (frame rates 10×30, 5×60, 5×120, and 10×240 s).

Data Analysis

The image analysis of dynamic PET was performed with Inveon Research Workplace 3.0 (Siemens, Knoxville, TN, USA). Region of interests (ROIs) were automatically delineated by a threshold algorithm in the target tissue on the last frame (@60 min) of dynamic PET images. The time-activity curves (TACs) were derived by superimposing the same ROI to each frame of the entire dynamic image series. The value of each time point on TAC represents the mean uptake of radioactive tracer in the ROI. As reported previously, two-tissue (three-compartment) model is the most appropriate model to characterize the specific binding process of RGD peptide [26]. Based on Logan graphical analysis with reference region [28], muscle was selected as the reference tissue because of its negligible integrin expression. The slope of the linear portion of the Logan plot is the distribution volume ratio (DVR). Consequently, the binding potential (BP$_{ND}$=k_3/k_4), a macro-parameter reflecting the binding affinity in vivo, can be derived from DVR (BP$_{ND}$=DVR−1).

Immunohistochemistry

After sacrificing the animals, tumor tissue was collected immediately. The sampled specimens were snap frozen in liquid nitrogen and stored at−70 °C until staining was performed. Frozen tumor tissues were sectioned (5 µm) and stained using the biotinylated monoclonal anti-α$_v$β$_3$ antibody. The following primary antibodies against different target antigens were used: anti-mouse CD31 antibody and anti-mouse CD61 antibody. After PBS washing, the slices were mounted with DAPI-containing mounting medium. The fluorescence images were acquired with an epifluorescence microscope (Olympus, X81). Subsequently, CD31- and CD61-positive areas were counted in five adjacent microscopic fields using a ×40 magnifying lens and a ×10 ocular lens, corresponding to an area of 0.588 mm^2. Determination of microvessel density and staining intensity was performed by one senior pathologist, who was blinded for the image quantification results.

Statistical Analysis

Static uptake (%ID/g) and BP$_{ND}$ parameters determined from PET were summarized as mean±SD. Differences between treated and control tumors were evaluated using unpaired Student t test. P values less than 0.05 were considered statistically significant. Similar comparison and statistical analysis were conducted on the parameters derived from static images and PET kinetic analysis.

Results

Effects of VEGF$_{121}$/rGel on Tumor Growth

To evaluate the effect of VEGF$_{121}$/rGel treatment on tumor growth, we monitored the tumor size throughout the study (Fig. 1b). As shown, the U87MG tumor growth was
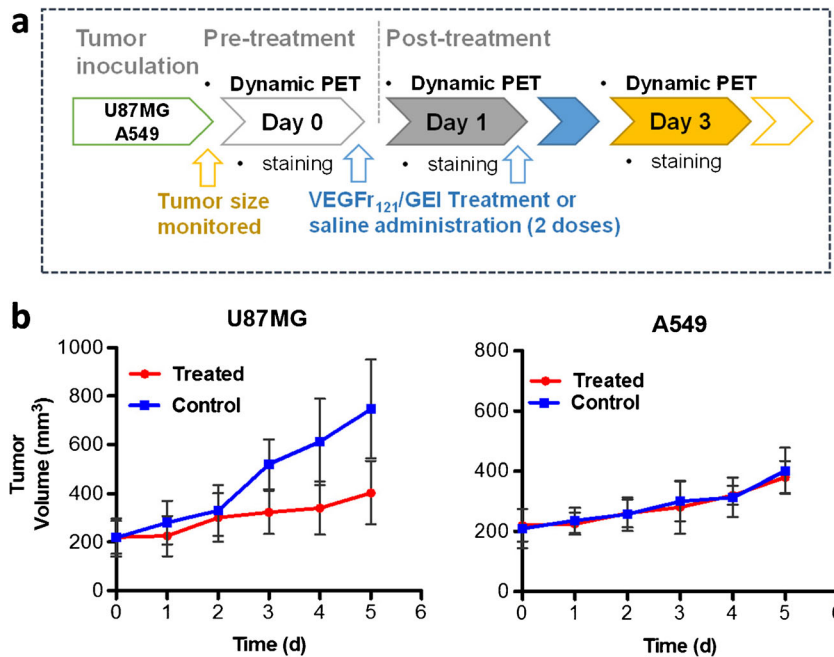
Fig. 1 a Study design. **b** Tumor growth curves for U87MG (*left*) and A549 (*right*) tumors for VEGF$_{121}$/rGel treatment and control groups.

obviously delayed after VEGF$_{121}$/rGel treatment, as compared to the control group. The growth-inhibiting effect became evident after day 3, which corroborates the previous findings [16]. The growth of A549 tumor, however, was not affected by VEGF$_{121}$/rGel administration.

Quantitative Evaluation

Representative PET static images and parametric maps (BP$_{ND}$) of U87MG-treated and control mice are presented in Fig. 2a–d, and the quantitative results are summarized in Fig. 2e, f. The U87MG tumor uptakes of [^{18}F]FPPRGD2 at 1-h time point were 5.40±1.26, 4.65±1.55, and 3.15±0.69 %ID/g on days 0, 1, and 3 for the treatment group, while those for the control group were 4.60±0.78, 4.90±1.36, and 6.07±1.21 %ID/g on days 0, 1, and 3, respectively. The tracer uptake (%ID/g) did not show significant difference between the treated and control tumors until day 3. For the kinetic parameter estimation, the BP$_{ND}$ values of U87MG tumors in the treatment group were 4.58±0.68, 3.65±0.15, and 2.14±0.73 on days 0, 1, and 3, while those in the control group were 4.87±0.54, 5.51±0.81, and 5.98±0.16 on days 0, 1, and 3, respectively. It is of note that significant difference in BP$_{ND}$ value was already found 1 day after VEGF$_{121}$/rGel treatment started ($P<0.05$), which became more significant on day 3 ($P<0.01$). BP$_{ND}$ maps showed significant decrease after treatment, which was more obvious than that observed from static tumor uptake (%ID/g). Comparing with the static images, the parametric maps show much

better tumor-to-background ratio for both treated and control groups.

The effect of VEGF$_{121}$/rGel on A549 tumors was also characterized by dynamic PET images and quantitative assessment. In Fig. 3, the tumor uptakes at 60 min of A549-treated group were 4.06±0.53, 3.54±0.28, and 3.39±0.89 on days 0, 1, and 3, respectively, which were similar to those of control group (4.01±0.85, 3.52±0.17, and 3.82±1.06 on days 0, 1, and 3). The BP$_{ND}$ values were 3.95±0.26, 3.47±0.29, and 3.53±1.04, while those of control subjects were 3.65±1.10, 3.78±0.09, and 3.71±0.36 on days 0, 1, and 3, respectively. There was no significant difference found between groups of A549. The tumor uptake of [^{18}F]FPPRGD2 and BP$_{ND}$ values in A549 groups were lower than those in U87MG tumors, indicating lower integrin expression in A549 tumors. Same as the representative images shown, neither %ID/g nor BP$_{ND}$ showed significant changes after the treatment as the fusion protein was ineffective in inhibiting A549 tumor growth.

Time-Activity Curves

As shown in Fig. 4, the mean TACs of both U87MG and A549 were summarized and compared. Different patterns of TACs were observed among groups. U87MG control showed rapid tracer accumulation in tumor during the first 10 min and dropped fast afterward until reached equilibrium (Fig. 4a). However, the A549 control group showed
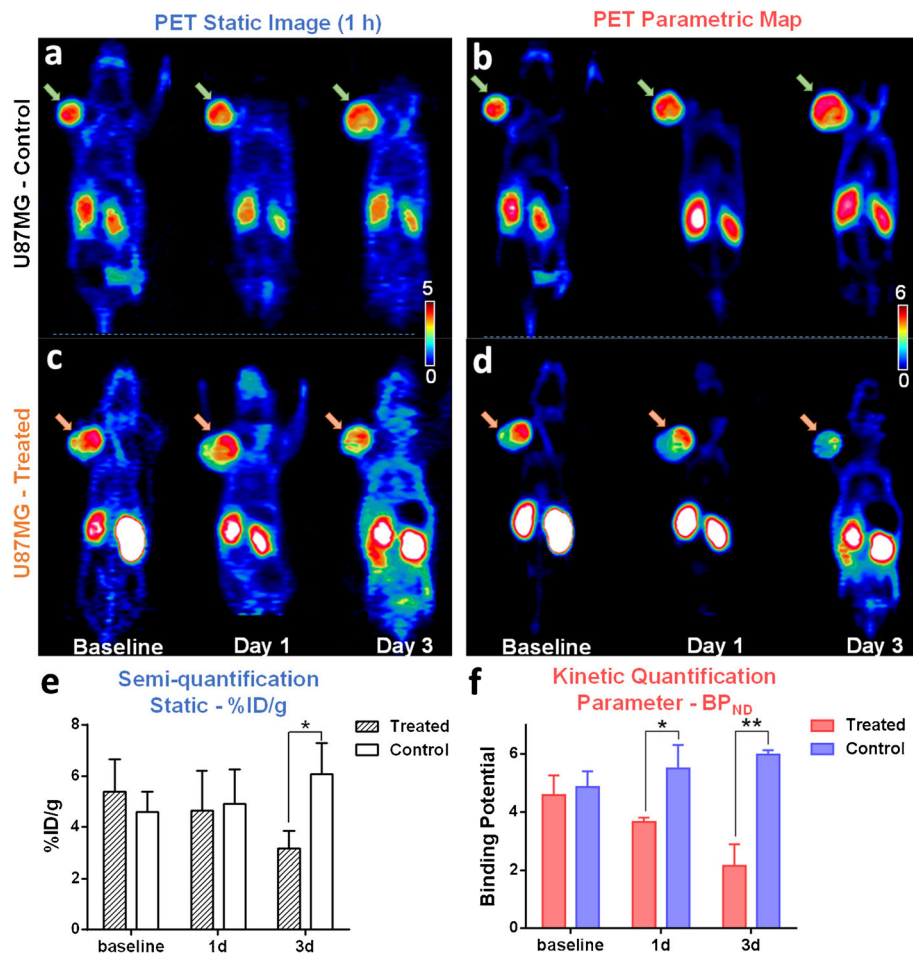
Fig. 2 Representative coronal images of U87MG-tumor-bearing mice with administration of VEGF$_{121}$/rGel (treated group) and PBS (control group) at baseline, day 1 and day 3 posttreatments. **a** The static PET images at 1 h after tracer injection and **b** parametric maps (BP$_{ND}$) derived from dynamic PET images for U87MG control group are presented. **c** The static PET images at 1 h and **d** parametric maps (BP$_{ND}$) for treated U87MG mice are presented. Quantitative analysis results, including **e** static tumor uptake @1 h shown as %ID/g and **f** kinetic parameter BP$_{ND}$ derived from dynamic PET analysis, are summarized.

relatively slow accumulation in tumor region and then reached a plateau 20 min after the tracer injection (Fig. 4b). The TAC peak of U87MG tumors (control) was significantly higher than that of A549 tumors (control), indicating that the highly vascularized U87MG tumors have better blood flow and permeability than A549. After treatment, the mean uptake of U87MG tumor decreased on day 1 and became more significant on day 3 as well as the slope of initial leading edge of TAC. The similar changes of TAC for A549 tumors were observed, but not as significant as those of U87MG tumors.

Microvessel Density and Integrin Expression

Immunofluorescence staining with CD31 and CD61 was conducted to further investigate the effects on tumor vasculature and integrin expression in blood vessels after

treatment. The U87MG tumors have abundant vasculature, as indicated by strong signal of CD31 staining of the untreated tumor slices (Fig. 5). Significant changes of vascular morphology as well as microvessel density were observed after VEGF$_{121}$/rGel treatment. Microvessel cavity was collapsed in treated U87MG tumor sections on day 1 and became extremely rare on day 3 after treatment. For A549 tumors, no difference in CD31 and CD61 staining was found between the treatment group and the control group (Fig. 6).

To further investigate the mechanism of altered RGD uptake due to the changes of integrin density and the specific targeting of the drug, we assessed the integrin expression with anti-human integrin $\alpha_v\beta_3$ antibodies. As shown in Supplementary material figures, both U87MG and A549 tumors had positive human integrin $\alpha_v\beta_3$ expression. Nevertheless, statistical analysis did not confirm a significant difference in the human integrin $\alpha_v\beta_3$ staining florescence intensity after treatment, indicating that the change of
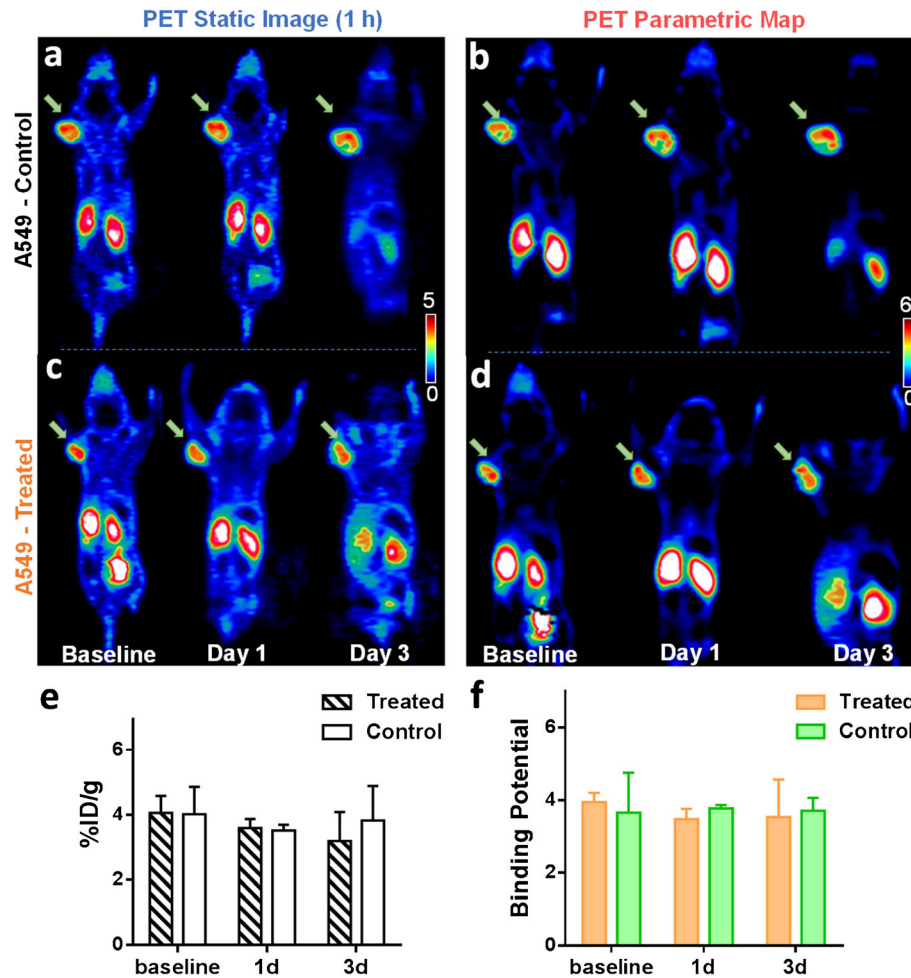
Fig. 3 Representative coronal images of A549-tumor-bearing mice with administration of VEGF$_{121}$/rGel (treated group) and PBS (control group) at baseline, day 1 and day 3 posttreatments. **a** The static PET images at 1 h after tracer injection and **b** parametric maps (BP$_{ND}$) derived from dynamic PET images for A549 control group are presented. **c** The static PET images at 1 h and **d** parametric maps (BP$_{ND}$) for treated A549 mice are presented. Quantitative analysis results, including **e** static tumor uptake @1 h shown as %ID/g and **f** kinetic parameter BP$_{ND}$ derived from dynamic PET analysis, are summarized.

tumor uptake of RGD and BP$_{ND}$ was not related to integrin expression on tumor cells but to the tumor vasculature.

Discussion

In recent years, quantitative analysis using kinetic analysis in PET imaging showed an increasing value in the tumor diagnosis as well as in tumor therapy assessment by providing indicative kinetic parameters which better characterize the *in vivo* biological processes. In therapy monitoring, the kinetic parameters derived from dynamic PET image series bring benefits to measure the specific therapeutic effect comparing with visual assessment and semiquantitative analysis usually used in clinic [29]. In this study, we tested the feasibility of applying dynamic PET imaging and quantitative analysis to evaluate the efficacy and early response of the treatment targeting tumor neovascularization using VEGF$_{121}$/rGel. Previous study reported that VEGF$_{121}$/

rGel is specifically cytotoxic to cells overexpressing VEGFR-2 (KDR) rather than those overexpressing VEGFR-1 (FLT-1) [4] and is internalized only into endothelial cells expressing VEGFR-2 but not VEGFR-1 [30]. However, it was confirmed that the level of VEGFR-2 expression varies in different individual tumors and even in the same tumor at different developmental stages [13]. Thus, in clinical setting, the early response monitoring is critical to determine the available candidates for specific targeted cancer therapy and adjust the treatment plan for those not responsive to it. To mimic the real clinical setting, we tested two tumor models U87MG and A549, which are highly and moderately vascularized, respectively [24, 25]. Furthermore, we applied dynamic imaging and kinetic modeling to delineate the specific therapeutic effect and thus further improve the sensitivity of treatment response evaluation.

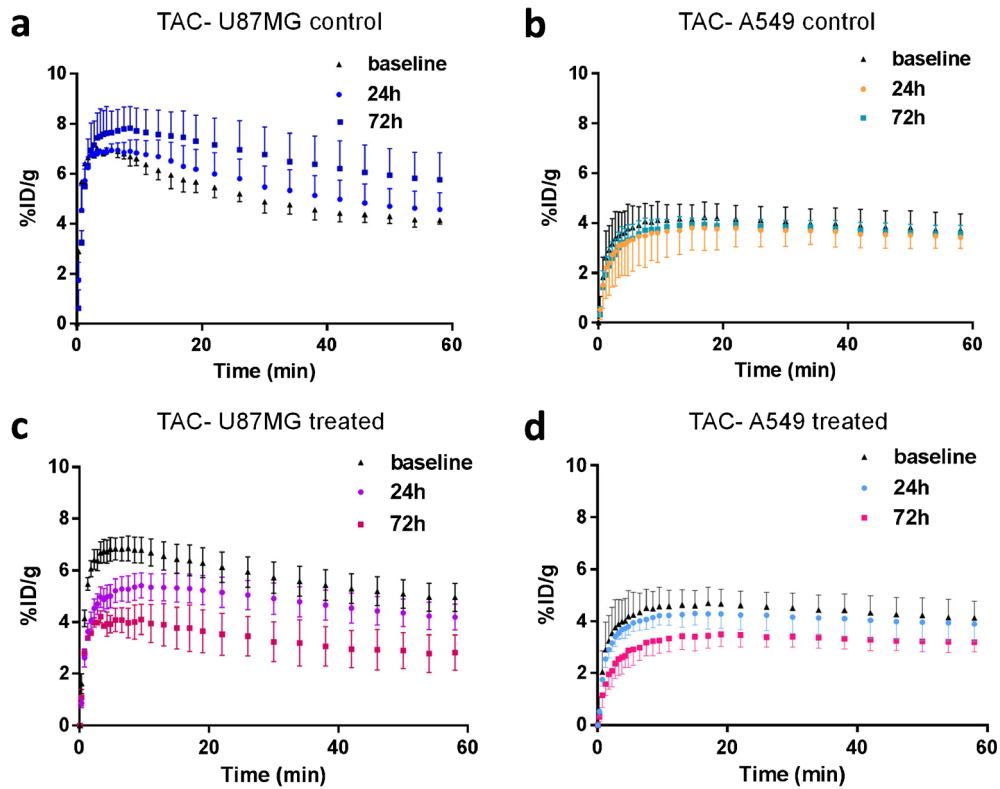Laufer *et al*. [31] used photoacoustic imaging to demonstrate that destruction phase in the posttreatment

Fig. 4 Mean time-activity curves of **a** U87MG and **b** A549 control groups, as well as the treated groups **c** U87MG and **d** A549 are shown (*N*=4).

changes within the tumor can be characterized by rapid vascular shutdown and extensive vessel disintegration, which resulted in strongly decreased perfusion particularly at the tumor core as well as increased hypoxia and cell death. In our study, the destruction and recovery of tumor vasculature may introduce a complicated impact on the flow and permeability that cancels the effect of each other and consequently reduces the sensitivity after the first day of
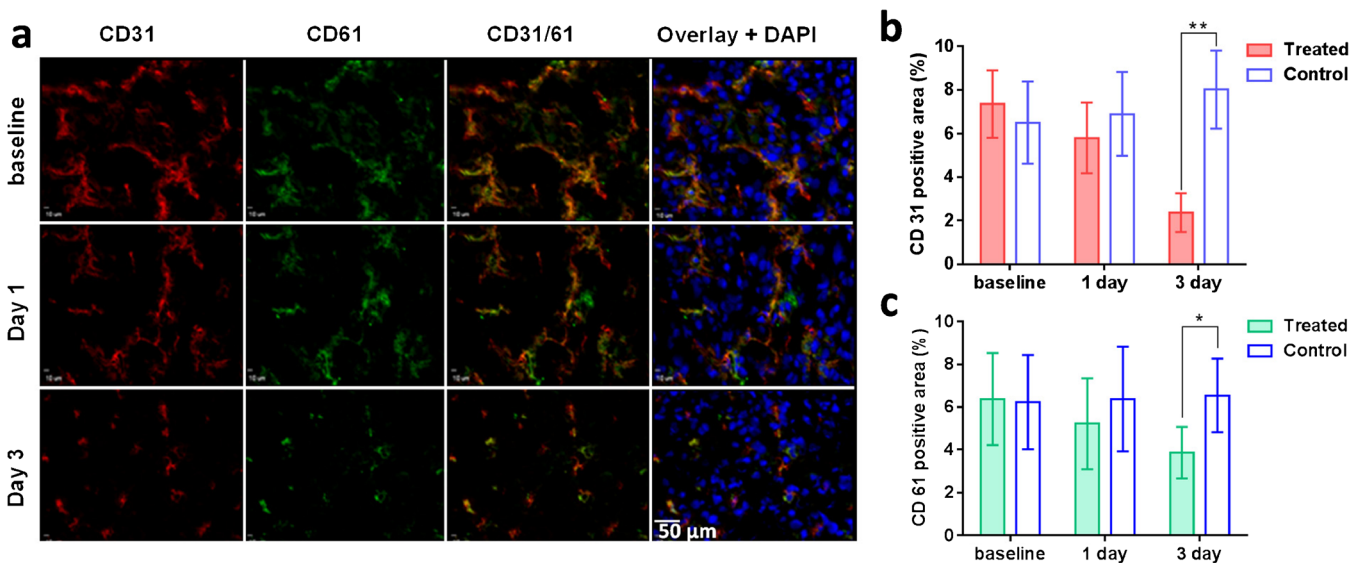

Fig. 5 **a** Immunofluorescence staining of U87MG tumor vasculature and murine integrin β_3 expression (tumor vasculature related): CD31 (*red*), CD61 (*green*), overlay of CD31/61, and overlay of CD31/61 plus DAPI (*blue*). **b** Calculated vascular area based on CD31 staining. **c** Integrated CD61 optical density. *$p<0.05$, **$p<0.01$.
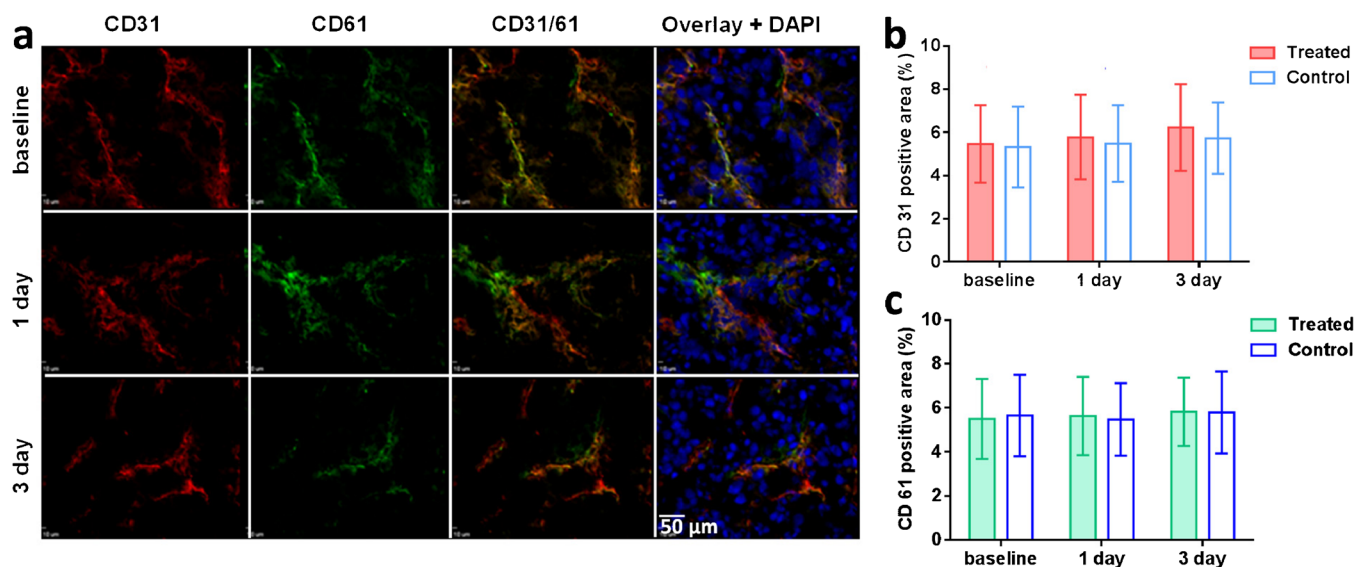
Fig. 6 a Immunofluorescence staining of A549 tumor vasculature and murine integrin β_3 expression (tumor vasculature related): CD31 (*red*), CD61 (*green*), overlay of CD31/61, and overlay of CD31/61 plus DAPI (*blue*). b Calculated vascular area based on CD31 staining. c Integrated CD61 optical density.

treatment. It is generally believed that the dysfunction of tumor vasculature induced by VDAs can cause nonspecific accumulation of PET radiotracer in the tumor region as well as slower elimination from the blood. Static PET image only gave a snapshot of the entire tumor region at a given time point. Thus, tumor uptake derived from static image was usually not sufficient to tell whether the tracer retention was due to the vasculature damage or through specific binding. Basically, $VEGF_{121}$/rGel treatment reduced vessel density and integrin expression, and therefore, specific binding of $[^{18}F]FPPRGD2$ in the tumor region would be decreased. However, complications from nonspecific tumor accumulation of $[^{18}F]FPPRGD2$ and slowed clearance from the blood led to insignificant difference in observed tumor uptake (%ID/g) at 1 day after treatment. At day 3, when the integrin expression and specific binding of $[^{18}F]FPPRGD2$ further reduced, difference in tumor uptake derived from static PET images became statistically significant. By applying the kinetic analysis, the BP_{ND} can eliminate the bias mentioned above and maximize the specific binding information that is the specific indicator for therapy response. Thus, although the U87MG tumor showed similar uptake of $[^{18}F]FPPRGD2$ as compared to the control group, the kinetic analysis observed significant reduction in BP_{ND} at 1 day after $VEGF_{121}$/rGel treatment. Our results suggested that the dynamic PET and kinetic parameters yield more sensitive estimation of early response to treatment compared with semiquantification from static images.

To the best of our knowledge, this is the first experiment using kinetic parameter to quantitatively analyze treatment response of tumors to a vascular-disruptive agent. More importantly, it demonstrated the feasibility of this novel approach to the early assessment of treatment response to molecular therapy, which is a significant unmet clinical need. Although we only showed the potentials of this new approach to the $VEGF_{121}$/rGel treatment, it should be able to apply to many other neovascularization targeting therapies. In the future, we will investigate the effectiveness of this approach to other vasculature-targeted therapies and the combination of such therapy regimen with chemotherapy and radiotherapy.

Depending on the image quantification results which were further confirmed by immunofluorescence staining, the U87MG tumor is responsive while A549 is nonresponsive to $VEGF_{121}$/rGel treatment. It is likely that KDR expresses at insufficient level to cause $VEGF_{121}$/rGel binding and vascular damage in A549 tumors [23]. We can only speculate on the reasons for different response of U87MG and A549 to the treatment, because we did not perform the VEGR-2 staining, which is a limitation of this study. However, the CD31 and CD61 staining results showed the tumor vasculature and murine integrin expression which confirmed our speculation of why U87MG is more responsible to the VDA treatment. And, the TAC results generally reflect the different patterns of blood flow and permeability which are consistent with the immunohistochemical results. To further reveal the mechanism of treatment response in tumors, VEGR-2 staining and quantitative analysis would be performed which is beyond the range of this study.

Conclusions

Quantitative analysis based on dynamic PET with RGD peptide tracer shows advantages in distinguishing effective from ineffective treatment during the course of $VEGF_{121}$/rGel therapy at early stage and therefore provides more sensitive assessment than static PET.

Electronic supplementary material

Below is the link to the electronic supplementary material.ESM 1(PDF 2291 kb)

References

1. Li J, Sun Z, Zhang J et al (2011) A dual-targeting anticancer approach: soil and seed principle. Radiology 260:799–807
2. Thorpe PE (2004) Vascular targeting agents as cancer therapeutics. Clin Cancer Res 10:415–427
3. Tozer GM, Kanthou C, Baguley BC (2005) Disrupting tumour blood vessels. Nat Rev Cancer 5:423–435
4. Ran S, Mohamedali KA, Luster TA et al (2005) The vascular-ablative agent VEGF121/rGel inhibits pulmonary metastases of MDA-MB-231 breast tumors. Neoplasia 7:486–496
5. Zhang X, Lin Y, Gillies RJ (2010) Tumor pH and its measurement. J Nucl Med 51:1167–1170
6. Hsu AR, Cai W, Veeravagu A et al (2007) Multimodality molecular imaging of glioblastoma growth inhibition with vasculature-targeting fusion toxin VEGF121/rGel. J Nucl Med 48:445–454
7. Spear MA, LoRusso P, Mita A, Mita M (2011) Vascular disrupting agents (VDA) in oncology: advancing towards new therapeutic paradigms in the clinic. Curr Drug Targets 12:2009–2015
8. LeCouter J, Moritz DR, Li B et al (2003) Angiogenesis-independent endothelial protection of liver: role of VEGFR-1. Science 299:890–893
9. Ferrara N, Chen H, Davis-Smyth T et al (1998) Vascular endothelial growth factor is essential for corpus luteum angiogenesis. Nat Med 4:336–340
10. Carmeliet P, Jain RK (2011) Molecular mechanisms and clinical applications of angiogenesis. Nature 473:298–307
11. Ebos JM, Kerbel RS (2011) Antiangiogenic therapy: impact on invasion, disease progression, and metastasis. Nat Rev Clin Oncol 8:210–221
12. Ferrara N, Hillan KJ, Gerber HP, Novotny W (2004) Discovery and development of bevacizumab, an anti-VEGF antibody for treating cancer. Nat Rev Drug Discov 3:391–400
13. Cai W, Chen X (2008) Multimodality molecular imaging of tumor angiogenesis. J Nucl Med 49(Suppl 2):113S–128S
14. Veenendaal LM, Jin H, Ran S et al (2002) *In vitro* and *in vivo* studies of a VEGF121/rGelonin chimeric fusion toxin targeting the neovasculature of solid tumors. Proc Natl Acad Sci U S A 99:7866–7871
15. Cai W, Chen K, Mohamedali KA et al (2006) PET of vascular endothelial growth factor receptor expression. J Nucl Med 47:2048–2056
16. Yang M, Gao H, Sun X et al (2011) Multiplexed PET probes for imaging breast cancer early response to VEGF$_{121}$/rGel treatment. Mol Pharm 8:621–628
17. Nielsen T, Wittenborn T, Horsman MR (2012) Dynamic contrast-enhanced magnetic resonance imaging (DCE-MRI) in preclinical studies of antivascular treatments. Pharmaceutics 4:563–589
18. Eisenhauer EA, Therasse P, Bogaerts J et al (2009) New response evaluation criteria in solid tumours: revised RECIST guideline (version 1.1). Eur J Cancer 45:228–247
19. Bohndiek SE, Kettunen MI, Hu DE et al (2010) Detection of tumor response to a vascular disrupting agent by hyperpolarized 13C magnetic resonance spectroscopy. Mol Cancer Ther 9:3278–3288
20. Michalski MH, Chen X (2011) Molecular imaging in cancer treatment. Eur J Nucl Med Mol Imaging 38:358–377
21. Tomasi G, Turkheimer F, Aboagye E (2012) Importance of quantification for the analysis of PET data in oncology: review of current methods and trends for the future. Mol Imaging Biol 14:131–146
22. Muzi M, O'Sullivan F, Mankoff DA et al (2012) Quantitative assessment of dynamic PET imaging data in cancer imaging. Magn Res Imaging 30:1203–1215
23. Chatterjee S, Heukamp LC, Siobal M et al (2013) Tumor VEGF:VEGFR2 autocrine feed-forward loop triggers angiogenesis in lung cancer. J Clin Invest 123:1732–1740
24. Smrekar B, Wightman L, Wolschek MF et al (2003) Tissue-dependent factors affect gene delivery to tumors *in vivo*. Gene Ther 10:1079–1088
25. de Bouard S, Herlin P, Christensen JG et al (2007) Antiangiogenic and anti-invasive effects of sunitinib on experimental human glioblastoma. Neuro Oncol 9:412–423
26. Guo N, Lang L, Li W et al (2012) Quantitative analysis and comparison study of [^{18}F]AlF-NOTA-PRGD2, [^{18}F]FPPRGD2 and [^{68}Ga]Ga-NOTA-PRGD2 using a reference tissue model. PLoS One 7, e37506
27. Lang L, Li W, Guo N et al (2011) Comparison study of [^{18}F]FAl-NOTA-PRGD2, [^{18}F]FPPRGD2, and [^{68}Ga]Ga-NOTA-PRGD2 for PET imaging of U87MG tumors in mice. Bioconjug Chem 22:2415–2422
28. Logan J, Fowler JS, Volkow ND et al (1996) Distribution volume ratios without blood sampling from graphical analysis of PET data. J Cereb Blood Flow Metab 16:834–840
29. Takesh M (2012) The potential benefit by application of kinetic analysis of PET in the clinical oncology. ISRN Oncol 2012:349351
30. Mohamedali KA, Ran S, Gomez-Manzano C et al (2011) Cytotoxicity of VEGF$_{121}$/rGel on vascular endothelial cells resulting in inhibition of angiogenesis is mediated via VEGFR-2. BMC cancer 11:358
31. Laufer J, Johnson P, Zhang E et al (2012) *In vivo* preclinical photoacoustic imaging of tumor vasculature development and therapy. J Biomed Opt 17:056016